JOURNAL OF Materials CHEMISTRY

Mesomorphic and photoconductive properties of a mesogenic long-chain tetraphenylporphyrin nickel(II) complex

Hirosato Monobe, Shoji Mima, Takushi Sugino and Yo Shimizu*

Department of Organic Materials, Osaka National Research Institute, AIST, METI, 1-8-31 Midorigaoka, Ikeda, Osaka 563-8577, Japan. E-mail: yo@onri.go.jp

Received 13th November 2000, Accepted 26th January 2001
First published as an Advance Article on the web 12th March 2001

A tetraphenylporphinatonickel-based mesogenic compound 5,10,15,20-tetrakis(4-*n*-pentadecylphenyl)porphinatonickel(II) (C_{15}TPPNi) was synthesised and its mesomorphic and photoconductive properties were investigated. The photoconductive properties were compared with those of the metal-free compound. All measurements were carried out for symmetrical ITO/C_{15}TPPNi/ITO type cells and steady-state currents in the constant temperature conditions were detected. A photocurrent rectification was seen in either the crystal phase or lamellar mesophase of C_{15}TPPNi. The metal-free compound with pentadecyl chains showed a strong dependence of photocurrent rectification on mesomorphic phases: the rectification is shown in the cell of crystal and low-temperature lamellar phases and it disappears in the high-temperature lamellar mesophase. This phenomenon was interpreted in terms of the various mechanisms of charged carrier generation with the phase transition, based on the results of the action spectra and the illumination light intensity dependence of the photocurrent. The improvement of the contact for electric conduction at the interface upon heating was found, which is a special feature of this mesomorphic phase in the ITO/C_{15}TPPNi/ITO cell in comparison with the metal-free compound.

1. Introduction

The physicochemical properties of metalloporphyrins have been extensively studied during the last three decades from a biomimetic viewpoint.[1,2] The porphyrin skeleton has an extended π-conjugation system with 24 π-electrons leading to a wide range of wavelengths for light absorption and p-type properties as an electronic system. The analogous chlorophyll, in particular, is well-known to play an important role in photosynthetic processes and some metalloporphyrins show a remarkable photovoltaic effect in cells with the appropriate structure.[3–6] These indicate that metalloporphyrins have some potentiality for electronic charge transportation and excited energy migration.[7]

However, these properties derived from the electronic state of a molecule are subject to the metal species inserted in the central core. Sometimes they are likely to show a drastic change of electronic properties in their molecular aggregations. Thus, a well-designed molecular architecture of porphyrins could realise a variety of high performance functional properties if the self-assembled structure is well controlled.[8,9]

On the other hand, mesogenic compounds are one of the most interesting categories of self-assembled systems from these points of view. In particular, discotic liquid crystals are strongly expected to show high order anisotropic properties for electronic charge carrier transportation as well as energy migration because of their characteristic structures such as columnar mesophases.[6,10,11] Several disc-shaped mesogens derived from a porphyrin skeleton have been reported so far.[7] However, as for the mesomorphic behaviour of tetraphenylporphyrin and its metal complexes, only a few reports have been published to reveal the occurrence of unfamiliar mesophases such as the so-called 'discotic lamellar mesophase', which have layered structures formed by disc-shaped molecules and are just like smectic mesophases of rod-like molecules.[12] The details of these lamellar mesophases have not been clarified yet, though some variations of molecular arrangements for discotic lamellar phases are expected. However, this complicated situation of discotic lamellar mesophases is showing a few interesting features for their potential in charged carrier migration. The lamellar mesophases exhibited by a series of long-chain metallotetraphenylporphyrins tend to show very high viscosity, indicating the high molecular order of aggregations which was evidenced by several reflection peaks in the wide angle region of their X-ray diffraction patterns. This fact, in other words, indicates that the lamellar mesophases of tetraphenylporphyrin mesogens may have some effective structures appropriate for charge migration and/or electronic hopping in their mesomorphic structure.

In 1986, the first report about the photocurrent behaviour was published for an ITO sandwich-type cell into which a long-chain tetraphenylporphyrin without any metal ions in the central core, the metal-free derivative, was injected.[13] The phase transition dependence of the photocurrent on the positive electrode illumination clearly showed a marked increase of photocurrent at the crystal–lamellar phase transition, while at the phase transition between two lamellar mesophases the photocurrent stepwise decreases. Furthermore, the *V–I* characteristics of photocurrent exhibit remarkable rectification behaviour for both crystal and low-temperature lamellar phases, though it disappears at the phase transition between the low- and high-temperature lamellar mesophases, which is the first report of an intermesophase transition dependence of photocurrent rectification for a cell using a mesophase material. Several attempts have been made to explain this phenomenon in terms of various mechanisms of photocarrier generation in the cell on the phase transitions.[13–17]

In this work, a new long-chain metallotetraphenylporphyrin, 5,10,15,20-tetrakis(4-*n*-pentadecylphenyl)porphinatonickel(II), abbreviated as C_{15}TPPNi, was synthesised and its mesomorphic phase transition behaviour was investigated. This complex is interesting in terms of photoconductivity because its molecular arrangement is different from that of the metal-free compound probably due to the non-coplanarity of the tetraphenylporphyrin skeleton arising from the short Ni–N

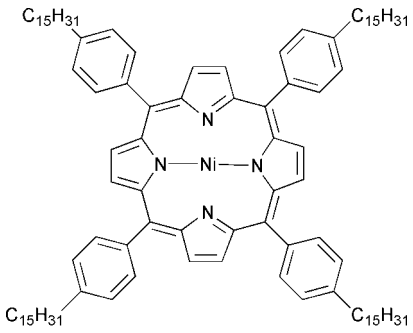

C_{15}TPPNi

Scheme 1 Chemical structure of C_{15}TPPNi.

bond.[10] Furthermore, some photoconduction properties were studied for a symmetrical ITO/C_{15}TPPNi/ITO cell.

2. Experimental

2.1. Compounds

Synthesis and purification of a mesogenic nickel tetraphenylporphyrin complex were carried out according to a well-known method with slight modifications. Formylation of *n*-pentadecylbenzene[18] and the following cyclization reaction of the resultant *n*-pentadecylbenzaldehyde with pyrrole[19] gave the metal-free tetraphenylporphyrin derivative, 5,10,15,20-tetrakis(4-*n*-pentadecylphenyl)porphyrin ($C_{15}TPPH_2$). The nickel(II) complex was synthesised from $C_{15}TPPH_2$ and a larger molar excess of $NiCl_2$.[20] The details are described as follows.

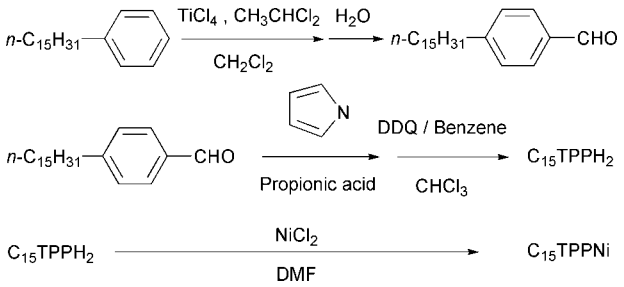

Scheme 2 Synthesis procedure of C_{15}TPPNi.

4-*n*-Pentadecylbenzaldehyde was prepared with a slight modification of a formylation method by Reiche *et al.*[18] *n*-Pentadecylbenzene (12.25 g, 42.5 mmol, Tokyokasei) was dissolved into 60 ml of dried dichloromethane and the solution was cooled on ice. $TiCl_4$ (16.77 g, 88.4 mmol) was added into the solution and 1,1-dichloromethyl methyl ether (4.70 g, 40.9 mmol) was added dropwise with vigorous stirring below 10 °C. The solution was stirred for 30 minutes on an ice bath and for 45 minutes at room temperature. The reaction mixture was poured into 500 ml of ice-cold water and stirred for more than 30 minutes. The yellow organic layer was separated from the aqueous layer and was washed by distilled water three times to be dried on anhydrous Na_2SO_4. Evaporation of solvent gave an orange oily liquid. The crude product was purified by column chromatography with silica gel using hexane at first, then a hexane–benzene (4 : 1) mixture, as eluents. The *para*-derivative was treated with activated carbon in methanol solution and finally recrystallised from hexane to give 6.95 g (25.3 mmol) of 4-*n*-pentadecylbenzaldehyde (yield: 51%). ^{1}H-NMR (500 MHz, $CDCl_3$, δ in ppm): 0.87 (t, 3H, CH_3), 1.24 (m, 24H, $(\underline{CH_2})_{12}CH_3$), 1.63 (quintet, 2H, $C_6H_4CH_2\underline{CH_2}$), 2.67 (t, 2H, $C_6H_4\underline{CH_2}$), 7.32 (d, 2H, *ortho* to the phenyl carbon attached to the alkyl chain), 7.78 (d, 2H, *meta*), 9.95 (s, 1H, CHO). IR (KBr) ν_{max}/cm^{-1} 1680 (C=O str.).

$C_{15}TPPH_2$ was synthesised by the method of Adler *et al.*[19] with slight modifications. 4-*n*-Pentadecylbenzaldehyde (12.47 g, 45.4 mmol) and the equimolar pyrrole (3.05 g, 45.4 mmol) were mixed in 120 ml of propionic acid and the mixture was refluxed for 30 minutes. After cooling to room temperature, the black solution was filtered to give dark violet solids. Washing with acetone gave clear violet crystals with metallic lustre. The chlorine derivative obtained as a by-product of the cyclization reaction was oxidised to the corresponding tetraphenylporphyrin according to the literature.[21,22] The crude product was dissolved in 50 ml of ethanol-free chloroform and 2,3-dichloro-5,6-dicyano-4-benzoquinone (DDQ) (1.12 g, 4.92 mmol) in 90 ml of benzene was added. The solution was refluxed for 3 hours. Purification of the product was carried out twice by column chromatography [(i) neutral activated alumina, Merck active I using chloroform as eluent, (ii) neutral alumina, Merck active II–III using benzene as eluent], followed by recrystallisation from benzene–acetone (1 : 9). 1.4 g of violet crystals with metallic lustre were obtained (yield: 8.5%). ^{1}H-NMR (500 MHz, $CDCl_3$, δ in ppm): −2.72 (s, 2H, NH), 0.90 (t, 12H, CH_3), 1.33 (m, 80H, $(\underline{CH_2})_{10}CH_3$), 1.48 (quintet, 8H, $C_6H_4CH_2CH_2CH_2\underline{CH_2}$), 1.56 (quintet, 8H, $C_6H_4CH_2CH_2\underline{CH_2}$), 1.91 (quintet, 8H, $C_6H_4CH_2\underline{CH_2}$), 2.94 (t, 8H, $C_6H_4\underline{CH_2}$), 7.54 (d, 8H, *meta* to the phenyl carbon attached to the *meso* position of the porphyrin ring), 8.12 (d, 8H, *ortho* to the phenyl carbon attached to the *meso* position of the porphyrin ring), 8.86 (s, 8H, β position of the pyrrole). IR (KBr) ν_{max}/cm^{-1}: 3545 (NH str.). λ_{max} (ε_{max})/nm (l mol^{-1} cm^{-1}) (benzene): 421 (566000), 484 (4600), 517 (21000), 552 (11600), 593 (6100), 649 (5600).

The metal complex C_{15}TPPNi was synthesised according to the literature.[19] The corresponding metal-free porphyrin $C_{15}TPPH_2$ (0.50 g, 0.344 mmol) and a larger molar excess of $NiCl_2$ (0.407 g, 3.16 mmol) were mixed in 68 ml of *N,N*-dimethylformamide and the solution was refluxed for 6 hours. After cooling at room temperature and then in a refrigerator overnight, the solution was filtrated to give a solid and washing with acetone gave red-violet crystals with metallic lustre. Purification of the product was carried out by column chromatography (neutral activated alumina, Merck active I using chloroform as eluent) and recrystallised from benzene–acetone (1 : 9) solution, followed by Soxhlet extraction with methanol for purification of the ionic species. 0.394 g of red-violet crystals with metallic lustre was obtained (yield: 72%). ^{1}H-NMR (500 MHz, $CDCl_3$, δ in ppm): 0.87 (t, 12H, CH_3), 1.27 (m, 80H, $(\underline{CH_2})_{10}CH_3$), 1.44 (quintet, 8H, $C_6H_4CH_2CH_2CH_2\underline{CH_2}$), 1.53 (quintet, 8H, $C_6H_4CH_2CH_2\underline{CH_2}$), 1.86 (quintet, 8H, $C_6H_4CH_2\underline{CH_2}$), 2.88 (t, 8H, $C_6H_4\underline{CH_2}$), 7.47 (d, 8H, *meta* to the phenyl carbon attached to the *meso* position of the porphyrin ring), 7.90 (d, 8H, *ortho* to the phenyl carbon attached to the *meso* position of the porphyrin ring), 8.75 (s, 8H, β position of the pyrrole). λ_{max} (ε_{max})/nm (l mol^{-1} cm^{-1}) (benzene): 420 (263000), 530 (19700). Elemental analysis of $C_{104}H_{148}N_4Ni$ (1512.95): found (calculated): C 82.58 (82.56), H 10.14 (9.86), N 3.57 (3.70%).

2.2. General measurements

FT-IR spectra were measured using a Perkin Elmer Paragon1000 spectrometer. UV-visible absorption spectra were recorded using a Shimadzu UV-2500PC spectrophotometer. ^{1}H-NMR measurements were carried out using a JEOL JNM-A50N FT-NMR spectrometer.

2.3. Measurements of mesophase behaviour

The phase transition behaviour was studied using a differential scanning calorimeter (DSC) (TA Instruments, 2920 MDSC)

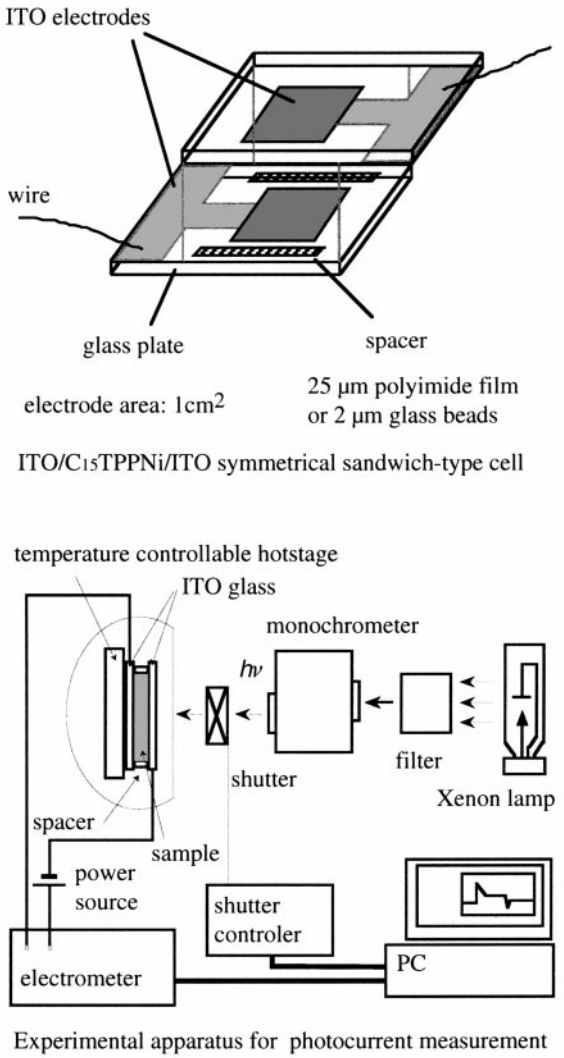

Fig. 1 Schematic diagram of the circuit and configuration of a sandwich type ITO/C_{15}TPPNi/ITO cell used for dark- and photo-current measurements.

with a mechanical cooling attachment and the texture was observed using a polarising microscope (Olympus, BH-2) equipped with a hot stage (Mettler, FP80HT). Powder X-ray diffraction studies were carried out by using a Rigaku Geigerflex X-ray diffractometer (CuKα) equipped with a handmade heating apparatus.

2.4. Measurements of photoconductivity

All measurements were carried out to obtain steady-state currents in the constant temperature conditions. Dark- and photo-currents were measured using the apparatus illustrated in Fig. 1. The sample cells were prepared using ITO-coated glass electrodes separated by 25 μm thick polyimide film or glass bead spacers with 2 μm diameter in parallel and fixed with silicon cement resulting in 29.4 and 4.2 μm thick cells, respectively. The effective area of the electrodes was adjusted to 1 cm^2 by etching of the ITO thin film. The cell thickness was evaluated by interferometry using a UV-visible spectrophotometer. C_{15}TPPNi was injected into the cell space by capillary action in the isotropic phase (*ca.* 130 °C) and the cell was cooled to room temperature very slowly (*ca.* 1 °C min^{-1}). Microscopic observation of the cell revealed that the thin film of C_{15}TPPNi was formed to have polydomain structures. Thus, all measurements in this work were for a polydomain film as shown in Fig. 2. The lamellar mesophase is highly viscous as suggested by X-ray diffraction studies and it was impossible to

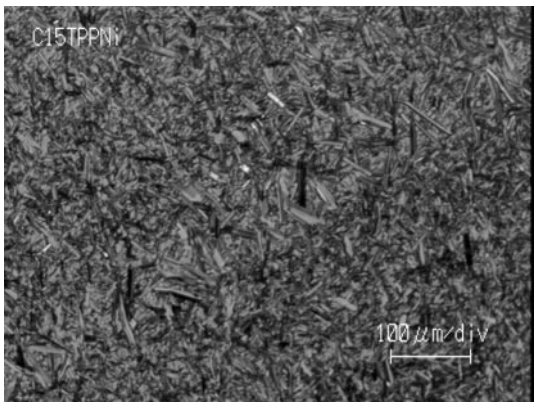

Fig. 2 Micrographic texture of a C_{15}TPPNi cell at 80 °C.

obtain a homogeneous monodomain film by modifying the cooling process. The electrical contact to the electrodes was attained using an electroconductive silver paste (Fujikurakasei, D-500) and copper wires. A 500 W xenon lamp (Ushio, UXL-500D) was used as the light source and the light was monochromated by a scanning monochrometer (Jasco, CT-10 and MS-25) to illuminate the sample cell in a temperature controllable cryostat under an inert atmosphere (Ar gas). The *V–I* characteristics of dark- and photo-currents were measured using a digital electrometer (Advantest, R8340) as a closed circuit under electric bias. The illumination light intensity was fixed to 0.34 mW cm^{-2} at 420 nm and 680 nm for all measurements. The temperature conditions were controlled to within 0.2 K using a temperature controller (Chino, SU10) and a cryostat (Oxford, Optistat). The positive carrier mobilities were measured by the TOF (time-of-flight) method. A Nd : YAG laser was used for pulsed light irradiation and the light wavelength was selected using an optical parametric oscillator (HOYA Continium, SURELITE II-10 and SURELITE OPO). The sample cell was set up in the cryostat and externally biased by a stabilised DC power supply. The transient photocurrent was detected by a digital oscilloscope (Iwatsu, DS9244) with a preamplifier (EG&G, 5185).

3. Results and discussion

3.1. Mesophase behaviour

Fig. 3a and b show DSC thermograms of C_{15}TPPNi at heating and cooling rates of 5 and 1 °C min^{-1}, respectively. On the first heating run (bottom), two endothermic peaks at 70 °C and 122 °C were detected. The clearing point was recognised at 122 °C by microscopic observation of the textures. On the second heating run, peaks appeared at 40 °C, 51 °C and 68 °C in Fig. 3a, and peaks at 42 °C and 67 °C, and a shoulder at 51 °C were detected in Fig. 3b. With the decrease of the exothermic peak at 54 °C on the second cooling run, the endothermic peaks at 40 °C and 51 °C were decreased and the crystal–mesophase transition peak at 68 °C was increased on the second heating run. These were probably induced by the formation of a metastable crystalline state in the cooling process at the different cooling rate. The thermodynamic parameters accompanying these transitions are listed in Table 1.

The results of powder X-ray diffraction measurements for the mesophase at 100 °C and for the crystal at 30 °C are shown in Fig. 4a and b, respectively. In the X-ray diffraction pattern of the mesophase on the wide angle region, the broad halo around $2\theta = 20°$ derived from the molten alkyl chains indicates this phase to be mesomorphic as shown in Fig. 4a. However, a few sharp reflections were also detected in the wide angle region which could be derived from the existence of a columnar structure in the smectic-like layer. Four peaks appear in the low angle region and these spacings are 34.0 Å, 17.0 Å, 11.3 Å, and

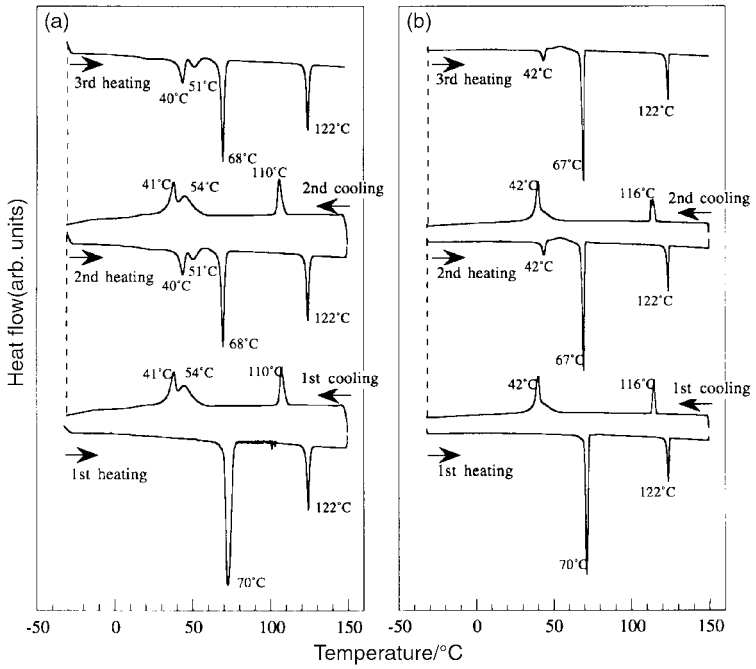

Fig. 3 DSC thermograms of C_{15}TPPNi. Heating and cooling rates were (a) 5 °C min^{-1} and (b) 1 °C min^{-1}, respectively.

8.1 Å. The ratio of these spacings is 1 : 1/2 : 1/3 : 1/4, characteristic of a so-called 'lamellar' structure. Another weak peak appears in the low angle region at the spacing of 22.6 Å; the ratio between this peak and first one is 1 : $1/\sqrt{2}$, characteristic of a tetragonal arrangement of Ni ions which is centred in the porphyrin ring. On the other hand, three peaks appear in the low to wide angle region and these spacings are 9.50 Å, 4.55 Å and 3.16 Å. This suggests that molecular stacks of columns exist in the layer. The results indicate that this phase is like a crystal but is still a lamellar type mesophase, M_{LC}. There are slight differences in the X-ray diffraction patterns between Fig. 4a and b. Several additional peaks appear in the crystal phase at 30 °C as shown in Fig. 4b. However, the peaks corresponding to a layered structure remained as in the mesophase. This means the structural change on the M_{LC} to crystal phase transition is rather small.

C_{15}TPPNi shows one mesophase, a M_{LC} phase, between the crystal and the isotropic phases, while the corresponding metal-free compound shows two lamellar-type mesophases, a M_L and a M_{LC} phase. The lamellar phase which was exhibited by C_{15}TPPNi is the low-temperature lamellar mesophase in the metal-free compound which is close to the crystal phase. The stability of the Ni complex is lower than that of the metal-free compound probably due to the non-coplanarity of nickel porphyrin induced by a twist of the square planar geometry.[1,9]

Table 1 Thermodynamic quantities for the phase transitions of C15TPPNi

		T/°C (ΔH/kJ mol^{-1})					
Sample	Mode	Cr_0–M_{LC}		M_{LC}–I			
Recrystallisation from solution	1st heating	70	(104)	122	(23)		
		Cr_2–Cr_1		Cr_1–M_{LC}		M_{LC}–I	
Melt-grown		40	(19)	68	(47)	122	(24)

3.2. Photocurrent action spectra

Fig. 5 shows the absorption spectra of an ITO/C_{15}TPPNi/ITO cell and a benzene solution. There were no significant differences between the spectral patterns. The absorption of the cell at wavelengths smaller than 340 nm is due to the absorption of ITO electrodes. Also, no changes of the band maxima were observed through the crystal and mesophase in the Soret band near 420 nm and the Q band around 530 nm.

Fig. 6 and 7 show the photocurrent action spectra for positive and negative electrode illumination for 29.4 and

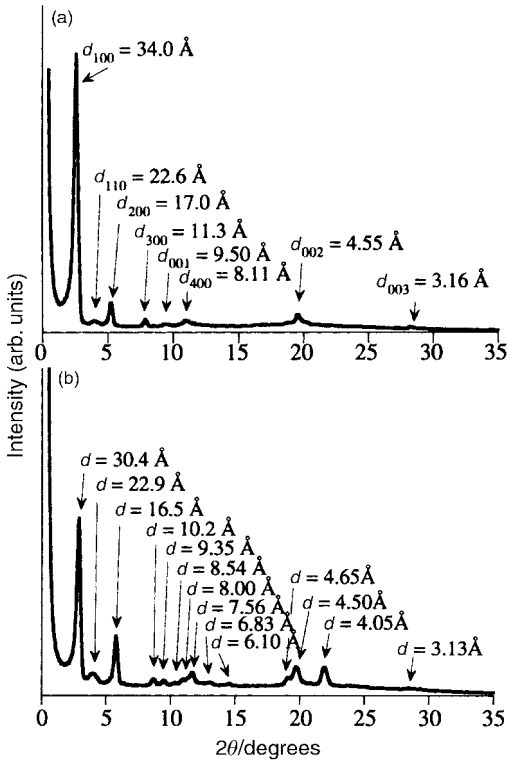

Fig. 4 X-Ray diffraction patterns (powder) of C_{15}TPPNi (non-oriented) at (a) 105 °C in the mesophase and (b) 30 °C in the crystalline phase.

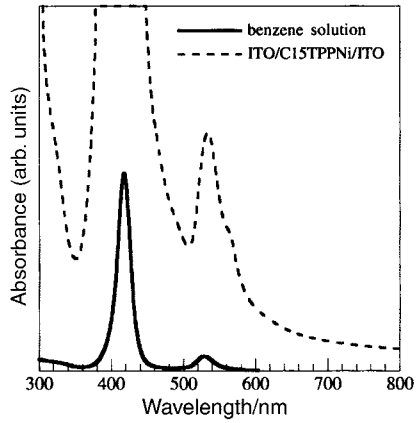

Fig. 5 Absorption spectra of a C_{15}TPPNi film sandwiched between glass plates (2.8 μm thick) and a benzene solution.

4.2 μm thick cells, respectively. These were measured at room temperature (crystalline state), the lower temperature region (80 °C) and the higher temperature region (110 °C) of the M_{LC} phase.

For the positive electrode illumination of the crystalline cell with 29.4 μm thickness, the spectral pattern in the longer wavelength region does not coincide with the absorption spectrum, showing an antibatic relation, and in the shorter wavelength region corresponding to the Soret band the photocurrent is very small. This indicates that most of the hole carriers generated near the interface are trapped and/or recombined during the transportation. Thus, the photocurrent observed is derived from the carriers generated in the bulk region. This could explain the antibatic relation between the

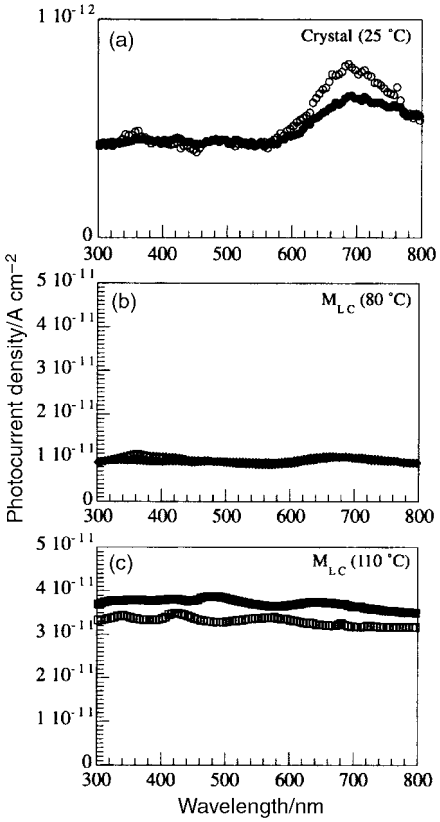

Fig. 6 Action spectra for the positive (solid line) and negative (dotted line, relieved in white) electrode illumination of a 29.4 μm thick ITO/C_{15}TPPNi/ITO cell for (a) the crystal (30 °C; ●), (b) the lower temperature region of M_{LC} (80 °C; ⧫) and (c) the higher temperature region of M_{LC} (110 °C; ■) phases. Bias: 8000 V cm^{-1} (actual applied voltage 23.52 V), light intensity: 0.34 mW cm^{-2}.

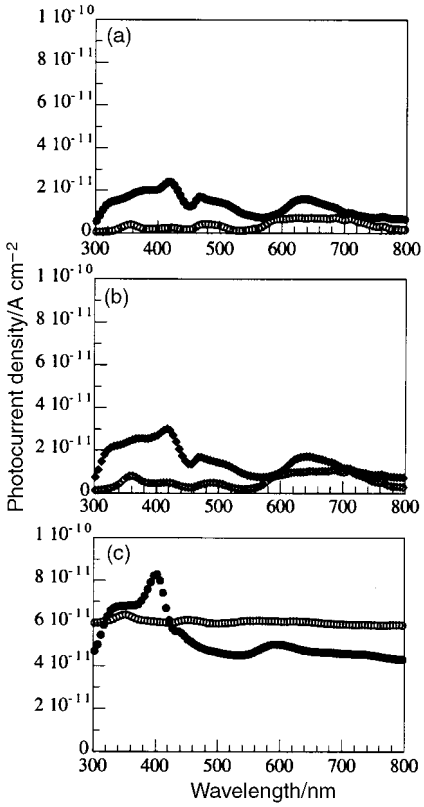

Fig. 7 Action spectra for the positive (solid line) and negative (dotted line, relieved in white) electrode illumination of a 4.2 μm thick ITO/C_{15}TPPNi/ITO cell for (a) the crystal (30 °C; ●), (b) the lower temperature region of M_{LC} (80 °C; ⧫) and (c) the higher temperature region of M_{LC} (110 °C; ■) phases. Bias: 8000 V cm^{-1} (actual applied voltage 3.33 V), light intensity: 0.34 mW cm^{-2}.

action and absorption spectra in the longer wavelength region where the compound has a lower absorption coefficiency. In addition, the spectral pattern for the negative electrode illumination of the crystalline cell was similar to that for the positive one. In the lower and higher temperature regions of the M_{LC} phase, the same patterns were seen except for the enhanced photocurrent in the crystal phase.

In the longer wavelength region, the spectral pattern for a 29.4 μm thick cell shows an antibatic relation to the absorption spectrum of an ITO/C_{15}TPPNi/ITO cell, though a symbatic relation can be seen for a 4.2 μm thick cell in the shorter wavelength region. This result strongly indicates that the photoconductive phenomena of the cell are related to the bimolecular recombination process and the charged carrier generation process near the electrode interface as well as in the bulk region.

The relation of illumination light intensity I_0 to current density j is expressed as shown in eqn. (1);[23] this enabled us to speculate that the carrier generation process contributed to the observed photocurrent, where e is the electronic charge, μ the effective carrier mobility, E the electric field, n the average concentration of charge carriers, d the film thickness, η the photocarrier quantum yield, I_0 the incident photon flux per unit area, α the absorption coefficient, and γ the recombination coefficient in the model. According to this equation, a symbatic relation between j and α is predicted for small values of αd and an antibatic one for large values of αd.

$$j = ne\mu E = 2e\mu/d(\eta I_0/\alpha\gamma)^{0.5}[1 - \exp(-\alpha d/2)]E \qquad (1)$$

As for the action spectra of the 4.2 μm thick cell, complex spectral patterns were observed as shown in Fig. 7. While the spectra for the negative electrode illumination were almost antibatically related to the absorption spectra in all phases,

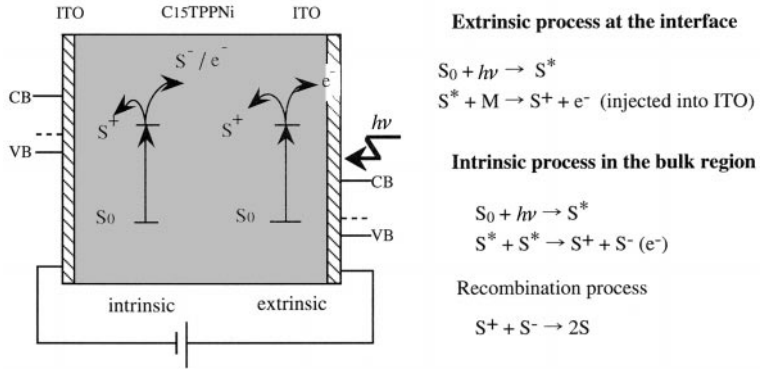

Fig. 8 A schematic representation of the proposed charged carrier generation mechanisms in a sandwich type ITO/C_{15}TPPNi/ITO cell.

those for the positive electrode illumination look like overlapped symbatic and antibatic spectra in the crystal and in the lower temperature region of the M_{LC} phase. In the higher-temperature region of the M_{LC} phase, the spectral patterns for both polarities of illumination look antibatic. These results indicate that an extrinsic mechanism contributes to the observed photocurrent for the positive electrode illumination in the crystal and the lower temperature region of the M_{LC} phase, in addition to an intrinsic one. In the higher-temperature region of the M_{LC} phase, however, it could be inferred that only intrinsic mechanism contributes to the observed photocurrent. In addition, the spectra for the negative electrode illumination show some complexity in which the patterns consist of mainly antibatic with some symbatic ones. In particular, a maximum of the photocurrent was observed between minima and maxima in the absorption spectrum, indicating that the illuminated light from the negative side might reach the interface on the counter electrode to generate carriers in an extrinsic way in the thinner cell.

This indicates that the observed photocurrent arises from (i) an extrinsic process performed at the interface between an ITO electrode and a mesogenic long-chain metallotetraphenylporphyrin and (ii) an intrinsic process working in the bulk region as shown in Fig. 8. This carrier generation situation is similar to the metal-free one.[15,16] In fact, Tanimura *et al*. reported that an electronic injection occurs from the exited tetraphenylporphyrin (non-peripheral alkyl chains) to the ITO electrode.[24] This injection phenomenon could act as a generation process of hole carriers in this system. Thus, it is reasonably thought that such an electronic injection similarly occurs at the interface between a mesogenic metallotetraphenylporphyrin and an ITO electrode, when the long-chain metallotetraphenylporphyrin is raised to the excited state by light absorption.

3.3. Light intensity dependence of photocurrent

On the other hand, it is well known that the current density j observed is related to the illumination light intensity I_0 as shown in eqn. (2) and the value of light exponent n varies depending on the charge carrier generation process.

Table 2 Light exponents depending on the charged carrier generation and transit processes of photoconduction for low intensity illumination

	Light exponent	
	Recombination	
Carrier number by one photon	limited	negligible
1	0.5	1.0
2	1.0	2.0

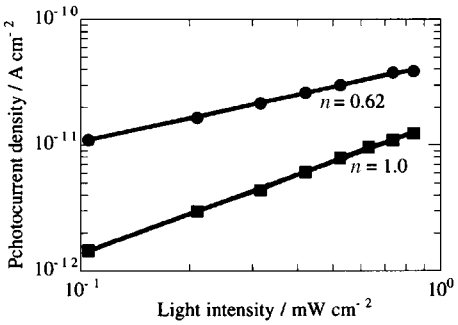

Fig. 9 Light intensity dependence of photocurrents for a 4.2 μm thick ITO/C_{15}TPPNi/ITO cell under 8000 V cm^{-1} electric bias and 420 nm light illumination for the positive (●) and negative (■) electrodes at room temperature.

$$j \propto I_0^n \tag{2}$$

These values are crucial for the photocarrier generation process and the carrier recombination in transit. The relation among the carrier generation, recombination and light exponent n is summarised in Table 2 for low intensity measurements.[25–27] Actually the values of light exponent were obtained by log-log plots of photocurrent *vs.* illumination light intensity, in which all plots exhibited well-defined straight lines to give the value n within the intensity region of the measurements as shown in Fig. 9. As for the case of the present cell, extrinsic and intrinsic processes are generating one carrier and two carriers by one photon absorption, respectively.

Table 3 shows the film thickness and the light wavelength dependence of light exponent values experimentally obtained at room temperature for both positive and negative electrode illumination. The light exponent values for positive electrode illumination appeared between 0.5 and 1, in contrast to almost unity of the exponent values for the negative electrode illumination. These results indicate that in the positive electrode illumination, the charge carrier contributing to the observed photocurrent is 'holes' generated by both extrinsic

Table 3 Film thickness dependence of light exponents in the positive and negative electrode illumination for a symmetrical ITO/C_{15}TPPNi/ITO cell

		Light exponent	
		Electrode illuminated	
Film thickness/μm	Wavelength/nm	positive	negative
4.2	420	0.62	1.0
	680	0.89	1.0
29.8	680	1.0	1.0

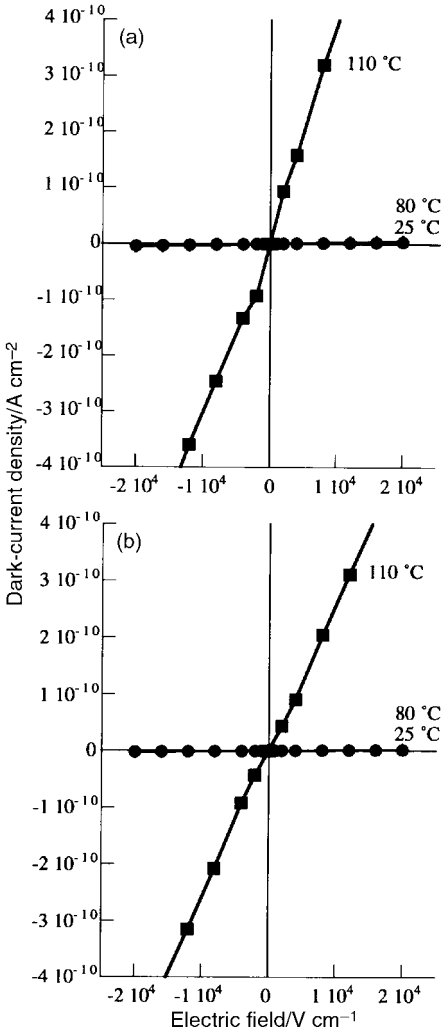

Fig. 10 Applied electric field dependence of dark-current for ITO/C_{15}TPPNi/ITO cells (a) 29.4 μm and (b) 4.2 μm thickness for the crystal (30 °C; ●), lower temperature region of M_{LC} (80 °C; ⧫) and higher temperature region of M_{LC} (110 °C; ■) phases of C_{15}TPPNi.

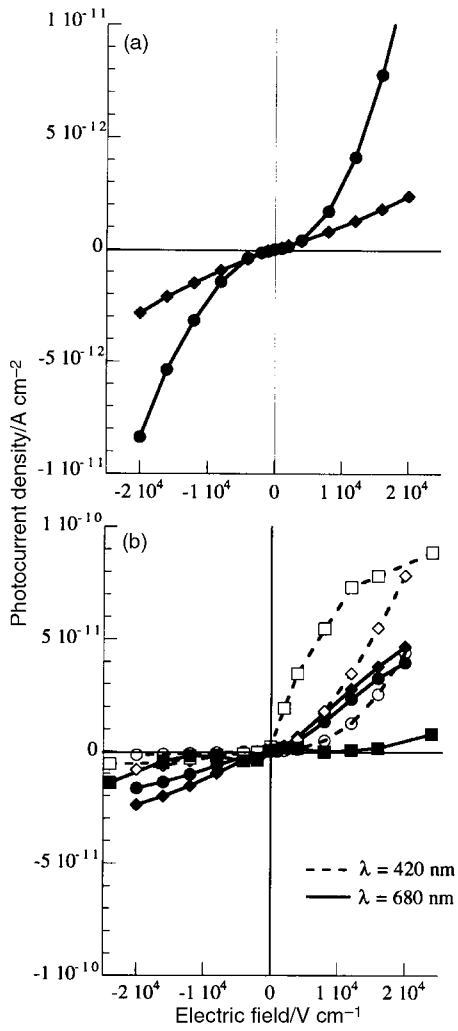

Fig. 11 Applied electric field dependence of photocurrents for ITO/C_{15}TPPNi/ITO cells (a) 29.4 μm and (b) 4.2 μm thick for the crystal (30 °C; ●), lower temperature region of M_{LC} (80 °C; ⧫) and higher temperature region of M_{LC} (110 °C; ■) under 420 nm (dotted line, relieved in white) and 680 nm (solid line) light illumination with an intensity of 0.34 mW cm^{-2}.

and intrinsic processes, though in the negative electrode illumination the carrier is generated only by the intrinsic process.

Table 4 shows the phase dependence of light exponent values experimentally obtained for both positive and negative electrode illumination of a 4.2 μm thick cell. The light exponent values for the positive electrode illumination appeared between 0.5 and 1, and the values increase as the temperature is elevated. This implied that the contribution of the extrinsic process for the observed photocurrent depends on the phase and it decreased with the crystal to M_{LC} phase transition as well as the temperature increase in the M_{LC} phase.

Table 4 Light exponents depending on the phase transitions of C_{15}TPPNi in a 4.2 μm thick ITO/C_{15}TPPNi/ITO cell under 420 nm light illumination

	Light exponent	
	Electrode illuminated	
Phase	positive	negative
Crystal (30 °C)	0.62	1.0
M_{LC} (80 °C)	0.89	1.0
M_L (110 °C)	1.0	1.0

3.4. Applied electric field dependence of dark- and photocurrents

Fig. 10 shows the dark-current *vs.* applied electric field characteristics of the ITO/C_{15}TPPNi/ITO cells; (a) 29.4 μm and (b) 4.2 μm thick cells for the crystal, the low temperature region of M_{LC} (80 °C) and the higher temperature region of M_{LC} (110 °C) phases for C_{15}TPPNi. Symmetrical features are clearly shown in the bias electric field of ± 20000 V cm^{-1}. The conductivity σ was calculated to be $\sim 10^{-15}\,\Omega^{-1}\,cm^{-1}$ for the crystal and the low temperature region of M_{LC} phases and $\sim 10^{-13}\,\Omega^{-1}\,cm^{-1}$ for the higher temperature region of the M_{LC} phase. The conductivity of C_{15}TPPNi is comparable with that of the free base, $C_{15}TPPH_2$, in any phases.

Fig. 11 shows the photocurrent *vs.* applied electric field characteristics of the cells at room temperature, 80 °C and 110 °C. Marked rectification of the photocurrent is apparent for both the crystal and M_{Lc} phase 4.2 μm thick cells, the positive electrode illumination causing a larger photocurrent which increases with the bias voltage, though symmetrical behaviour is observed for the M_{LC} phase 29.4 μm thick cell. The wavelength effect on the photocurrent is remarkable: see Fig. 11(b). In the case of illuminating light wavelength of 420 nm, corresponding to the Soret band absorption maximum, the photocurrent rectification is more remarkable than that at 680 nm which is a tail part of the Q-band absorption.

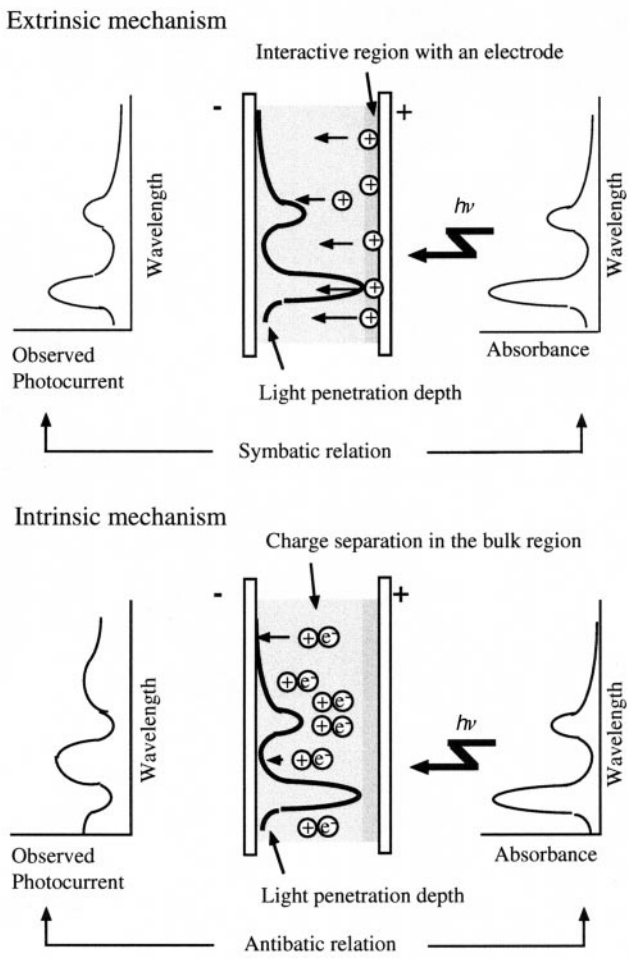

Fig. 12 Schematic representation of the carrier generation mechanism dependence of the observed photocurrent to the electrodes.

This phenomenon probably relates to the penetration depth of the illuminated light. The results indicate that the photoconductive phenomena of the cell are related to the bimolecular recombination process, the photocarrier generation process near the mesogen and electrode interface as well as in the bulk region and where the carriers transport toward the counter electrode (Fig. 12). It is a similar process to the case of metal-free $C_{15}TPPH_2$ in the M_{LC} phase.

Thus, the photocurrent rectification observed in the *V–I* (photocurrent) characteristics of the 4.2 μm thick cell, which could be seen for the crystal and M_{LC} phases, is mainly caused by the carriers generated by the extrinsic process of hole generation by an electron injection from the excited porphyrin to the ITO electrode. The extrinsic process occurs only for the positive electrode, leading to the rectification, and probably electron injection from the excited long-chain tetraphenylporphyrin to the ITO electrode is promoted by an applied electric field. Similar rectification behaviour was observed for the same type of cell using the analogous metal-free, Cu(II), and Zn(II) complexes having long chains.[13–16,28] For the same type of symmetrical cell using a mesomorphic Zn(II) porphyrin (octa-substituted), a similar mechanism of charged carrier generation was proposed in relation to the photovoltaic properties.[4]

It was revealed that a series of phase transitions for this compound do not cause any drastic changes to the lifetime of the singlet excited state of $C_{15}TPPH_2$, which varies within the range 8.5–10 ns through the crystal to M_L phase transitions, though it drops to 7 ns at the clearing point.[29] In the case of phthalocyanine solid films, it is known that their photocurrent behaviour is significantly sensitive to the molecular order of the films on the electrode surface. A crystal to M_{LC} phase

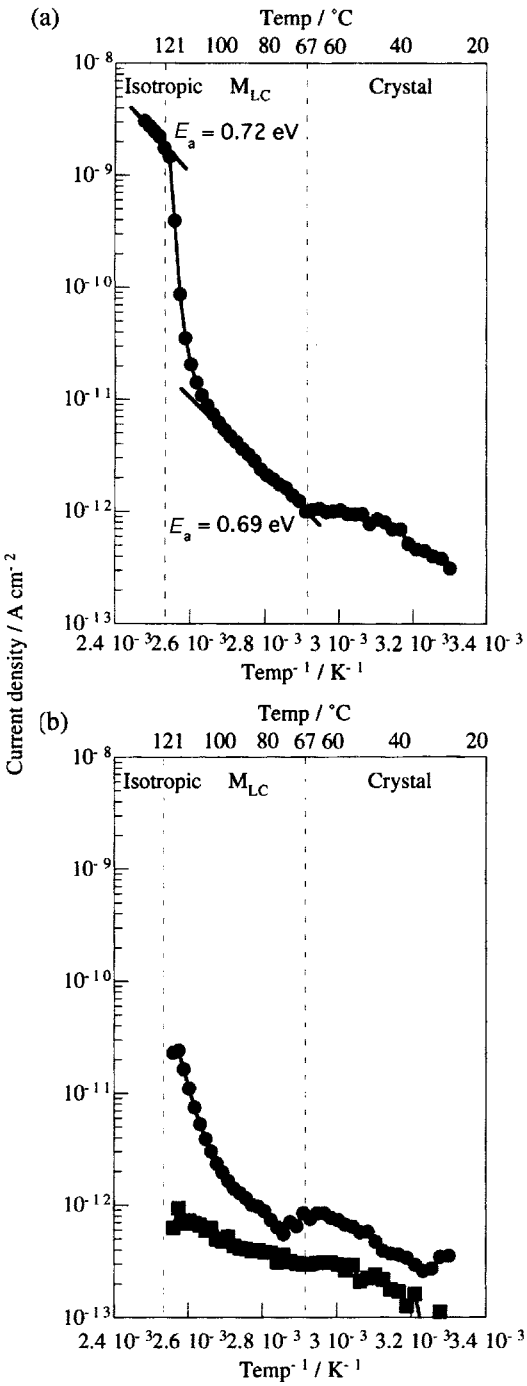

Fig. 13 Temperature dependence of (a) dark-current under 4000 V cm^{-1} and (b) photocurrent at 420 nm light illumination under 4000 V cm^{-1} electric bias, for the positive (●) and negative (■) electrode illumination of a 4.2 μm thick ITO/C_{15}TPPNi/ITO cell.

transition gives rise to changes not only of the molecular order, but also of the state of molecular fluctuation. The change of molecular order caused by this phase transition is inferred to be a change of the molecular stacking manner based on the XRD results. It would be reasonable to think that the molecular stacking is crucial for charge carrier hopping and the hopping probability is quite sensitive to the relative configuration of molecules, a manner of stacking as for the columnar structure. On the other hand, the change of fluctuational modes and degrees caused by mesomorphic phase transitions could affect the charge carrier hopping rate.[30] For the present cell using a mesomorphic compound, both changes of molecular ordering and molecular dynamics should be considered for the observed phenomena.

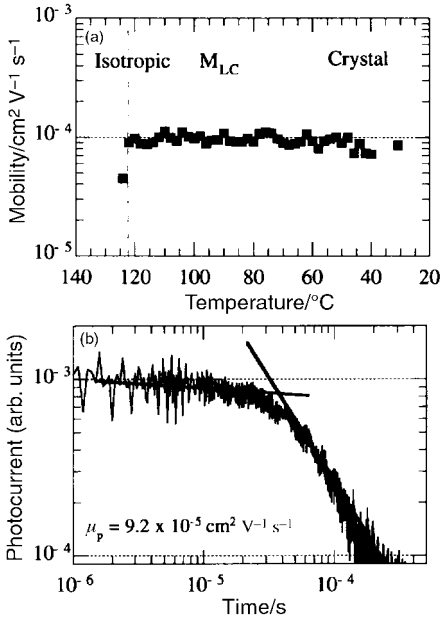

Fig. 14 (a) Temperature dependence of positive carrier mobility of C_{15}TPPNi. (b) A photocurrent transient in the M_{LC} (80 °C) phase for positive electrode illumination. Cell thickness: 4.2 μm, electric field: 1.2×10^5 V cm^{-1}, wavelength of pulse: 420 nm.

3.5. Temperature dependence of dark- and photo-currents and a positive carrier mobility

Fig. 13a and b show the dark- and photo-currents as a function of temperature for a 4.2 μm thick ITO/C_{15}TPPNi/ITO cell, respectively. The applied bias was 4000 V cm^{-1} (1.68 V), the illumination light wavelength was 420 nm and the light intensity was 0.34 mW cm^{-2}. The dark-current temperature dependence of the M_{LC} and isotropic phases obeyed the Arrhenius' equation in the low temperature range. The values of the activation energy for the conduction in each phase were calculated to be 0.69 eV and 0.72 eV for the M_{LC} and isotropic phases, respectively. In the higher temperature region of the M_{LC} phase, the dark-current was drastically increased. This could be explained by a pre-transition effect. It seems to be due to the additional contribution of ionic species to the current, probably a small amount of impurities or the generated hole molecules which could be transferable with the increase of molecular motion near the phase transition.

On the other hand, the photocurrent shows different behaviour from the dark-current. It behaves in a different manner between the positive and negative electrode illuminations. In positive electrode illumination, the photocurrent drastically increases upon heating the M_{LC} phase while there is a gradual increase in the crystal and M_{LC} phases for negative electrode illumination, followed by an undetectable level of photocurrent at the M_{LC} to isotropic phase transition for both cases. In the M_{LC} phase, the electronic conduction such as charge hopping is probably dominant as the charge migration process, rather than ionic conduction. Because of the high viscosity of the lamellar mesophase, it could not be thought that the charged porphyrin molecules themselves are able to easily migrate. Although there still remains the contribution of the ionic conduction for observed photocurrent as a increase of the temperature. We could expect two reasons that the hole conduction is dominant in ITO/C_{15}TPPNi/ITO cells. Firstly, the intrinsic defects are mainly p-type impurities, and secondly, the level of the work function of ITO is less than that for the metal-free system.

The current density j is proportionally dependent on the charged carrier number n, mobility μ and electric field strength E as shown in eqn. (3).

$$j = ne\mu E \quad (3)$$

According to the result of TOF studies as shown in Fig. 14, the positive carrier mobility is kept in the order of 10^{-4} cm^2 V^{-1} s^{-1} in the whole temperature range of the M_{LC} phase and hole conduction is dominant for the observed photocurrents. We could not evaluate the carrier mobility for negative charge because of the undetectable level of the transient photocurrent observed. The cell used for the mobility measurements was not a mono-domain film of the mesogen. The lamellar mesophase of C_{15}TPPNi has high viscosity and consequently it was difficult to obtain uniform alignment in the film as a large domain. Thus, the real mobility is, at least, faster than 10^{-4} cm^2 V^{-1} s^{-1}. It is also reported that the hole mobility is temperature independent in the mesomorphic phase in the case of triphenylene derivative discotic crystals with hexagonal arrays and the corresponding metal-free $C_{15}TPPH_2$.[31,32] In our case, positive carrier mobility was observed to be independent of the temperature. According to the recent works by Funahashi *et al.*, domain boundaries of conventional rod-like liquid crystalline systems essentially do not affect the charge migration efficiency and this is proposed to be a characteristic property of charge transportation in liquid crystals.[33,34] This implies that the surprising temperature-independent mobility change is a characteristic of the lamellar mesophase. The evaluated carrier mobility of the lamellar mesophase (10^{-4} cm^2 V^{-1} s^{-1}) was smaller than that in the hexagonal columnar phase for an alkylthiotriphenylene derivative (10^{-3} cm^2 V^{-1} s^{-1}) and that in more ordered structures such as the helical columnar phase (10^{-1} cm^2 V^{-1} s^{-1}).[11,35]

Therefore, this increase of photocurent could be mainly due to an increase of the effective number of charge carriers because the carrier mobility is independent of the temperature. This increase of photocurrent could be owing to the improvement of carrier transportation at the the domain–domain (in the bulk region) and the electrode–sample interfaces in the conduction process. In addition, the ionic conduction might contribute to the steady-state photocurrent with increasing temperature. The contact of a mesogenic material and a solid electrode which provides electric and ionic conduction pathways at the interfaces may have been improved by the molecular motion on heating (wetting). Although the fluctuations of the columnar structure are disadvantageous for electronic conduction, the advantage of molecular contact at the interfaces seems to be dominant for electric conduction in this ITO/C_{15}TPPNi/ITO system.

4. Conclusion

The action spectra and the applied electric field dependence of the photocurrent indicated that hole generation at the interface of the positive electrode is essential for the photocurrent rectification behaviour observed in the crystal and lamellar (M_{LC}) phases of C_{15}TPPNi. These phenomena may be related to the molecular order near the mesogen–electrode interface. In the case of the metal-free analogue, the photocurrent rectification was observed in the crystal and low-temperature lamellar phases and it disappears at the low-temperature lamellar (M_{LC}) to high-temperature lamellar (M_L) phase transition. This suggests that the lamellar mesophase which was exhibited in the C_{15}TPP Ni complex is the low-temperature lamellar phase in the metal-free compound which is close to the crystal phase. This is also supported by the X-ray diffraction results.

The dark- and photo-currents were increased on heating and it might be that electronic conduction rather than ionic conduction is dominant because the molecule is too large for ionic conduction in this highly viscous mesophase. Since the positive carrier mobility was retained in the M_{LC} phase, the

photocurrent increase arose from a increase of the number of carriers which was due to the better charge transportation at the interfaces. The contact of a mesogenic material and a solid electrode which provides electric and ionic conduction pathways at the interfaces was improved by the molecular motion on heating (wetting). We conclude that the improvement of the matching for conduction at the interface on heating is a special feature of this M_{LC} mesomorphic phase.

Acknowledgements

The authors acknowledge the Agency of Industrial Science and Technology (AIST), Ministry of International Trade and Industry of Japan (MITI) for the financial support under the national R&D project, "Harmonised Molecular Materials" operated in Industrial Science and Technology Frontier Program of AIST-MITI.

References

1 *The Porphyrins*, ed. D. Dolphin, Academic Press, New York, 1978, vol. I–VII.
2 *The Porphyrin Handbook*, ed. K. M. Kadish, K. M. Smith and R. Guilard, Academic Press, San Diego, 2000.
3 F. J. Kampas, K. Yamashita and J. Fajer, *Nature*, 1980, **284**, 40.
4 B. A. Gregg, M. A. Fox and A. J. Bard, *J. Phys. Chem.*, 1990, **94**, 1586.
5 T. Saito, S. Wada, T. Kobayashi, S. Suzuki and T. Iwayanagi, *J. Phys. Chem.*, 1993, **97**, 8026.
6 Z. D. Popvoic, *Chem. Phys.*, 1984, **86**, 311.
7 P. G. Schouten, J. M. Warman, M. P. de Haas, M. A. Fox and H.-L. Pan, *Nature*, 1991, **353**, 736.
8 *Metallomesogens—Synthesis, Properties and Applications*, ed. J. L. Serrano, Wiley-VCH, Weinheim, 1996.
9 N. Boden and B. Movaghar, in *Handbook of Liquid Crystals*, eds. D. Demus, J. W. Goodby, G. W. Gray, H. W. Spiess and V. Vill, Wiley-VCH, Weinheim, 1998, vol. 2B, ch. IX.
10 Y. Shimizu, M. Miya, A. Nagata, K. Ohta, I. Yamamoto and S. Kusabayashi, *Liq. Cryst.*, 1993, **14**, 735.
11 N. Boden, R. J. Bushby and J. Clements, *J. Chem. Phys.*, 1993, **98**, 5920.
12 D. Adam, P. Schumacher, J. Simmerer, L. Haussling, K. Siemensmeyer, K. H. Etzbach, H. Ringsdorf and D. Haarer, *Nature*, 1994, **371**, 141.
13 Y. Shimizu, A. Ishikawa and S. Kusabayashi, *Chem. Lett.*, 1986, 1041.
14 Y. Shimizu, A. Ishikawa, S. Kusabayashi, M. Miya and A. Nagata, *J. Chem. Soc., Chem. Commun.*, 1993, 656.
15 Y. Shimizu, T. Fuchita, T. Higashiyama and T. Sugino, *Mol. Cryst. Liq. Cryst.*, 1999, **331**, 575.
16 Y. Shimizu, T. Higashiyama and T. Fuchita, *Thin Solid Films*, 1998, **331**, 279.
17 Y. Shimizu, H. Monobe, S. Mima, T. Higashiyama, T. Fuchita and T. Sugino, *Mater. Res. Soc. Symp. Proc.*, 1999, **559**, 211.
18 A. Reiche, H. Gross and E. Höft, *Chem. Ber.*, 1966, **93**, 88.
19 A. D. Adler, F. R. Longo, J. D. Finarelli, J. Goldmacher, J. Assour and L. Korskaoff, *J. Org. Chem.*, 1967, **32**, 476.
20 A. D. Adler, F. R. Longo, F. Kampas and J. Kim, *J. Inorg. Nucl. Chem.*, 1970, **32**, 2443.
21 K. Rousseau and D. Dolphin, *Tetrahedron Lett.*, 1974, **48**, 4251.
22 G. H. Barnet, M. F. Hudson and K. M. Smith, *J. Chem. Soc., Perkin Trans. 1*, 1975, 1401.
23 G. Giro, J. Kalinowski, P. D. Marco, V. Fattori and G. Marconi, *Chem. Phys. Lett.*, 1993, **211**, 580.
24 K. Tanimura, T. Kawai and T. Sakata, *J. Chem. Phys.*, 1979, **45**, 2639.
25 R. F. Chaiken and D. R. Kearns, *J. Chem. Phys.*, 1966, **45**, 3966.
26 G. R. Johnston and L. E. Lyons, *Aust. J. Chem.*, 1970, **23**, 1571.
27 G. R. Johnston and L. E. Lyons, *Chem. Phys. Lett.*, 1968, **2**, 489.
28 Y. Shimizu and H. Nakayama, unpublished data.
29 Y. Shimizu and T. Higashiyama, *Proc. SPIE, Int. Soc. Opt. Eng.*, 1998, **3319**, 177.
30 J. Simmerer, B. Glüsen and W. Paulus, *Adv. Mater.*, 1996, **8**, 815.
31 D. Adam, T. Closs, D. Funhoff, D. Haarer, H. Ringsdorf, P. Schuhmacher and K. Siemensmeyer, *Phys. Rev. Lett.*, 1993, **70**, 457.
32 H. Monobe, S. Mima and Y. Shimizu, *Chem. Lett.*, 2000, 1004.
33 M. Funahashi and J. Hanna, *Appl. Phys. Lett.*, 1998, **73**, 3733.
34 M. Funahashi and J. Hanna, *Appl. Phys. Lett.*, 2000, **76**, 2574.
35 A. M. van de Craats, J. M. Warman, M. P. de Haas, D. Adam, J. Simmerer, D. Haarer and P. Schuhmacher, *Adv. Mater.*, 1996, **8**, 823.